Optimum Placement of DF Antenna Elements for Accurate DOA Estimation in a Harsh Platform Environment

Gangil Byun, *Student Member, IEEE*, Hosung Choo, *Senior Member, IEEE*, and Hao Ling, *Fellow, IEEE*

***Abstract*—This paper presents a systematic approach to the optimum placement of direction finding (DF) antennas in a harsh platform environment. A circular array with omni-directional elements is considered for azimuthal direction of arrival (DOA) estimation based on the multiple signal classification (MUSIC) algorithm. The element positions are optimized by the use of a genetic algorithm (GA) in conjunction with the FEKO electromagnetic simulator. The proposed approach is first tested with a generic platform shape. It is then extended to a more realistic military aircraft model with a strong scattering object. The optimized results show a significant performance improvement over the uniform circular array in both platform environments.**

***Index Terms*—Antenna placement, direction finding (DF) antenna, direction of arrival (DOA) estimation, genetic algorithm, multiple signal classification (MUSIC) algorithm, platform effect.**

I. Introduction

In ELECTRONIC warfare, a direction finding (DF) system is typically deployed on military aircraft to estimate the direction of an incoming signal. This is accomplished by equipping the system with an antenna array in order to compare the amplitude and phase difference of the port current induced on each array element [1]–[4]. Thus, the spacing between the elements is considered as an important design factor in determining an accurate direction of arrival (DOA). For instance, the estimation ambiguity increases when the spacing is greater than a half wavelength due to grating lobes. A narrow spacing, on the other hand, brings significant mutual coupling effects between the elements, which increases estimation error in practice. This problem becomes more acute when the array is mounted on a large and complex platform that causes additional platform effects, such as wave scattering, blockage, and coupling [5]–[8]. Significant efforts have been made by using calibration methods, based on electromagnetic (EM) simulation or measurement, to mitigate such platform effects [9]–[14]. However, the calibrated array manifold may not bring a significant accuracy improvement in the case of a non-line-of-sight (NLOS) source due to an insufficient received signal power level, which lowers the signal-to-noise ratio (SNR). Another approach that has been explored is the position optimization method for array elements [15]. By using the optimized positions, the array can increase the radiation gain in the NLOS directions in order to improve the SNR. Thus, such an approach has some advantages in increasing the calibration capability even for NLOS sources.

This paper presents a systematic approach for DF antenna placement in a harsh platform environment. In our approach, we take into account the electromagnetic behavior of actual array elements, as well as platform effects, by using the full-wave FEKO EM simulator [16]. DOAs are estimated by using a signal-subspace MUSIC algorithm. A genetic algorithm (GA) is then used as an optimizer to minimize the DOA estimation error. Optimized element positions of the GA are further compared with those of a random search to verify the suitability and efficiency of our approach. We first test our approach using a generic arc-wall shape to gain better physical insights on platform effects in terms of DF. The approach is then applied to a more realistic military aircraft model to demonstrate its utility. In both platform environments, we employ a circular array of eight omni-directional antennas operating in the VHF/UHF bands. The array manifolds of given element positions are obtained via the amplitude and phase of the current induced on each element. The average root mean square error (RMSE) for all DOA angles is computed for evaluation. Then, the RMSE of the given positions is compared with that of a uniform circular array (UCA). Parametric studies are further conducted for the evaluation of the optimized positions using various sizes of the platform. The results demonstrate that our approach is efficient for achieving accurate DOA estimation in a harsh platform environment.

II. Study of Platform Effects Using an Arc-Wall

A. Geometry and DOA Estimation

Fig. 1 shows the geometry of an arc-wall surrounding eight dipole antennas. This generic wall shape is used to study how the DOA estimation error is affected by the platform environment. The wall is assumed to be a perfect electric conductor, and its size is determined by the wall radius R_{wall} and the wall spread angle φ_{wall}, which is defined as the angle between the x-axis and the end of the wall. To construct various platform environments, we vary the wall spread angle from 0° to 180° at intervals of 22.5°. In each environment, DOAs are estimated for the sources located in the azimuth direction by using the signal-subspace MUSIC algorithm that is given by

Manuscript received November 27, 2012; revised April 22, 2013; accepted June 04, 2013. Date of publication June 17, 2013; date of current version August 30, 2013. This work was supported by the MSIP (Ministry of Science, ICT & Planning), Korea, under the ITRC (Information Technology Research Center) support program (NIPA-2013-H0301-13-2007) supervised by the NIPA (National IT Industry Promotion Agency).

G. Byun is with the Department of Electronics and Computer Engineering, Hanyang University, Seoul, Korea.

H. Choo is with the School of Electronic and Electrical Engineering, Hongik University, Seoul, Korea (e-mail: hschoo@hongik.ac.kr).

H. Ling is with the Department of Electrical and Computer Engineering, The University of Texas at Austin, Austin, TX 78712 USA.

Digital Object Identifier 10.1109/TAP.2013.2269132

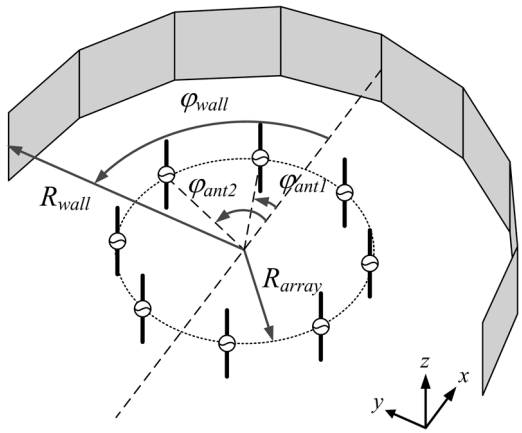

Fig. 1. Geometry of an arc-wall.

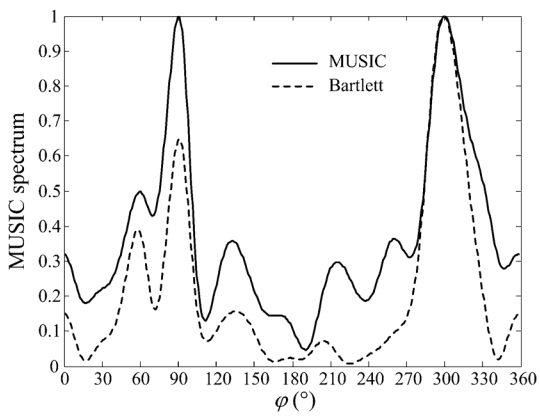

Fig. 2. Signal subspace MUSIC spectrum.

$$\overline{P}_{\text{signal}-\text{MU}}(\varphi) = \frac{\overline{a}^H(\varphi)\cdot\overline{U}_s\cdot\overline{U}_s^H\cdot\overline{a}(\varphi)}{\overline{a}^H(\varphi)\cdot\overline{a}(\varphi)} \tag{1}$$

where $\overline{a}^H(\varphi)$ indicates the conjugate transpose of the steering vector $\overline{a}(\varphi)$ at a given direction of φ. $\overline{U}_s$ is the signal subspace obtained via the eigenvalue decomposition of the covariance matrix $\overline{R}$, which is given by

$$\overline{R} = E\left(\overline{x}(t)\cdot\overline{x}^H(t)\right) \tag{2}$$

where $E(\cdot)$ is the expectation operator for the observations of K snapshots, and $\overline{x}(t)$ is the received signal that is obtained from the induced current at each array element terminated by 50 Ω. The received signal contains the source information as well as noise, as shown by

$$\overline{x}(t) = \overline{A}\cdot\overline{s}(t) + \overline{n}(t) \tag{3}$$

$\overline{A}$ is the array manifold matrix that represents a set of steering vectors, $\overline{s}$ is the signal vector, and $\overline{n}$ is the white Gaussian noise vector with a variance of σ^2. Note that this algorithm is related to the standard MUSIC algorithm by a simple algebraic transformation, given as

$$\overline{P}_{\text{noise}-\text{MU}}(\varphi) = \frac{1}{1-\overline{P}_{\text{signal}-\text{MU}}(\varphi)} \tag{4}$$

where the standard MUSIC is defined by:

$$\overline{P}_{\text{noise}-\text{MU}}(\varphi) = \frac{\overline{a}^H(\varphi)\cdot\overline{a}(\varphi)}{\overline{a}^H(\varphi)\cdot\overline{U}_n\cdot\overline{U}_n^H\cdot\overline{a}(\varphi)} \tag{5}$$

In (5), $\overline{U}_n$ is the noise subspace obtained from the same covariance matrix in (2). Although the standard MUSIC algorithm is widely used due to its super resolution characteristics [17], we use the signal-subspace MUSIC algorithm, whose spectrum is similar to a beamformer spectrum that distinctively reflects pattern variations distorted by nearby platforms. Fig. 2 shows a comparison between the signal-subspace MUSIC spectrum and the well-known Bartlett's beamformer spectrum [18]. These two patterns are obtained from an eight-element UCA with a radius of 0.75λ at 300 MHz. It is assumed that two vertically polarized sources, each with an incident power density of 6.27 mW/m at the center of the array, are independently located in the far field at $\varphi = 90°$ and $\varphi = 300°$. Horizontally polarized sources are not taken into account in this work, because the influence of depolarization due to diffraction caused by arc-wall edges is found to be small. The wall size is determined by the parameters of $\varphi_{\text{wall}} = 90°$ and $R_{\text{wall}} = 2.5$ m. In this platform environment, the Bartlett's spectrum shows a peak value of 0.63 in the direction of $\varphi = 90°$ due to the wave blockage effect caused by the presence of the wall. On the other hand, the signal-subspace MUSIC spectrum still maintains a value of 1.0 in the direction of $\varphi = 90°$. This is due to the normalization characteristics of the eigenvalue decomposition process [19], [20]. From this comparison, we see that the accuracy of the signal-subspace MUSIC algorithm is better than that of Bartlett's beamformer, when the spectrum is distorted by the platform effect. At the same time, the fact that the spectrum of the signal-subspace MUSIC is similar to that of a beamformer gives good insights on the effects of the platforms as compared to the standard MUSIC; since we can more readily observe the variations of the spectrum beamwidth and the side lobe levels (SLL).

B. GA Optimization

Fig. 3 shows the flow chart of our systematic approach to the antenna position optimization in a harsh platform environment. In our approach, GA is employed as an optimization algorithm to reduce the DOA estimation error. Initial chromosomes consisting of binary numbers are produced randomly to determine the coordinates of the array elements. We then excite a plane wave source in the same manner as in Fig. 2, at every 1° increment in the azimuth direction, and load each element port by 50 Ω to obtain the port current information induced by the sources. The array manifold of the simulated sample is calculated using the amplitude and the phase of the port current, and DOAs are estimated by the signal-subspace MUSIC algorithm. To evaluate each sample, the RMSE and the SLL are calculated respectively by (6) and (7)

$$RMSE = \sqrt{\frac{1}{M}\frac{1}{N}\sum_{f}\sum_{\varphi_{\text{source}}}\left|\varphi_{\text{est.}}(f)-\varphi_{\text{source}}\right|^2} \tag{6}$$

$$SLL = \frac{1}{M}\frac{1}{N}\sum_{f}\sum_{\varphi_{\text{source}}}\frac{P_{\text{side}}(\varphi_{\text{source}},f)}{P_{\text{main}}(\varphi_{\text{source}},f)} \tag{7}$$

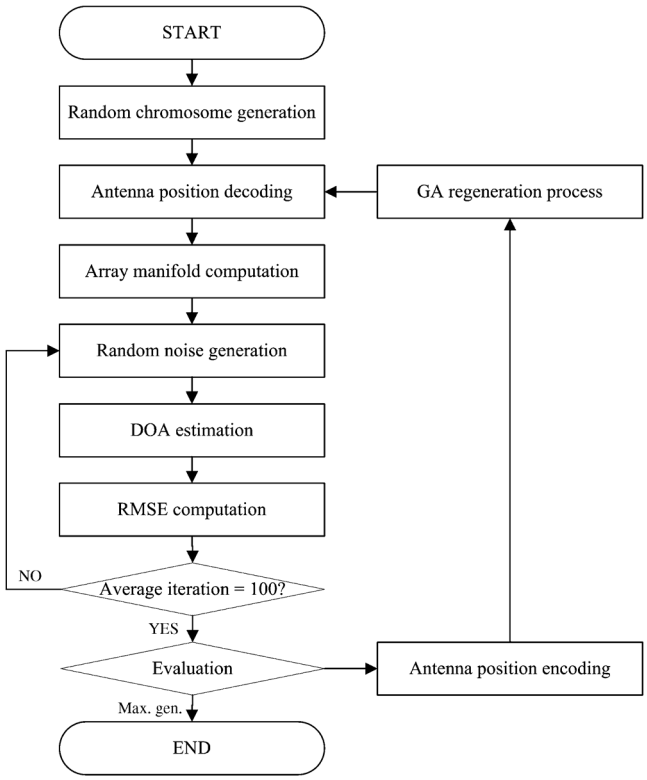

Fig. 3. Flow chart of our position optimization.

where $\varphi_{\mathrm{source}}$ is the source direction ($\varphi_{\mathrm{source}}$: $0°, 1°, \ldots, 359°$), and $\varphi_{\mathrm{est.}}$ is the estimated DOA. N is the number of source directions, and M is the number of frequency points (f: 200 MHz, 300 MHz, and 400 MHz). The SLL is calculated by dividing the peak value of the main lobe (P_{mainlobe}) into that of the peak side lobe (P_{sidelobe}). The estimation is conducted under the assumption that the SNR is 5 dB, and it is repeated one-hundred times to derive averaged values of RMSE and SLL in the presence of the random noise characteristic. The obtained average RMSE is used to evaluate the samples, and the average SLL is applied as a filtering condition so as to exclude some samples that have an average SLL of greater than 0.7. After evaluation, the coordinate information is encoded into binary numbers to apply it to the GA reproduction process of crossover and mutation [21]. The GA process is repeated for 25 generations, each of which consists of 40 populations. Thus, our GA process evaluates 1,000 samples in total to achieve a low RMSE. For a fair comparison, a random search (RS) is also carried out by evaluating 1,000 independent random samples with the same number of cost function evaluations. The best result is then chosen and compared against the GA result. The total computation time of both the GA and the RS is about 5 hours on a computer with an Intel Core i7-2600 quad-core processor and 16 GB of RAM. Since the GA should provide results better than the RS, this comparison allows us to evaluate the efficiency of the GA process.

C. Optimized Results

In our optimization, the array elements are symmetrically arranged with respect to the x-axis via their angular coordinates

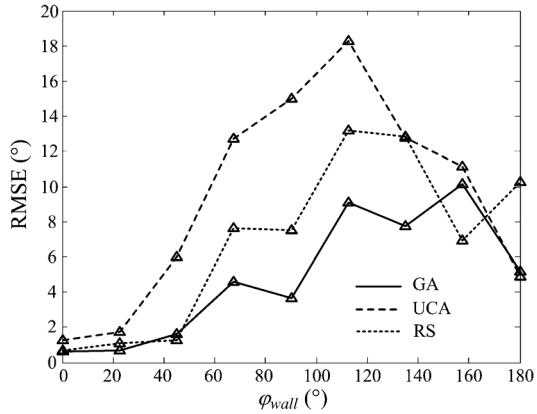

Fig. 4. Optimized RMSE according to φ_{wall}.

TABLE I
OPTIMIZED RESULTS OF THE ARC-WALL ($\varphi_{\mathrm{wall}} = 90°$)

Parameters	UCA	RS	GA
R_{array}	0.77 m	1.83 m	1.86 m
φ_{ant1}	22.5°	57°	128°
φ_{ant2}	67.5°	138°	143°
φ_{ant3}	112.5°	160°	155°
φ_{ant4}	157.5°	172°	174°
φ_{ant5}	202.5°	188°	186°
φ_{ant6}	247.5°	200°	205°
φ_{ant7}	292.5°	222°	217°
φ_{ant8}	337.5°	303°	232°

of $\varphi_{\mathrm{ant1}}, \varphi_{\mathrm{ant2}}, \ldots, \varphi_{\mathrm{ant8}}$ around a circle ($R_{\mathrm{array}}, 0.25$ m $\sim$ 2.00 m). The element spacing is set to be either uniform or nonuniform, which represents the UCA and the nonuniform circular array (non-UCA), respectively. Our approach is then applied to find the optimum value of R_{array} and the angular coordinates using the GA and the RS to determine the element positions.

Fig. 4 shows the optimized RMSE for different φ_{wall} values. The arc-wall is symmetrically formed at $R_{\mathrm{wall}} = 2.50$ m, and its coverage is adjusted by varying φ_{wall} from 0° to 180° at intervals of 22.5°. In the case of $\varphi_{\mathrm{wall}} = 0°$ (i.e., without any walls), the array configurations of both the UCA and the non-UCA (GA and RS, respectively) show a low RMSE of less than 2°. As the extent of the wall increases, the accuracy of the UCA is severely affected by platform effects. In contrast, the non-UCA optimized by GA does not exhibit a significant error increase for the entire range of φ_{wall}. For example, the RMSE of the GA is around 3.6° at $\varphi_{\mathrm{wall}} = 90°$, which is more than a factor of two smaller than that of the RS (7.5° at $\varphi_{\mathrm{wall}} = 90°$) and three times smaller than that of the UCA (15° at $\varphi_{\mathrm{wall}} = 90°$).

Table I shows the optimized parameters for $\varphi_{\mathrm{wall}} = 90°$, and Fig. 5(a) presents the optimized antenna positions from the GA. It is interesting to see that the antennas are clustered on the side away from the wall, but the element spacing is maintained at approximately 0.5λ at 300 MHz with the value of $R_{\mathrm{array}} = 1.86$ m. Fig. 5(b) shows the RMSE in the operating frequency range. We can also confirm that the GA shows consistently lower RMSE in the entire frequency band when compared to the other two results. Fig. 5(c) shows the RMSE ac-

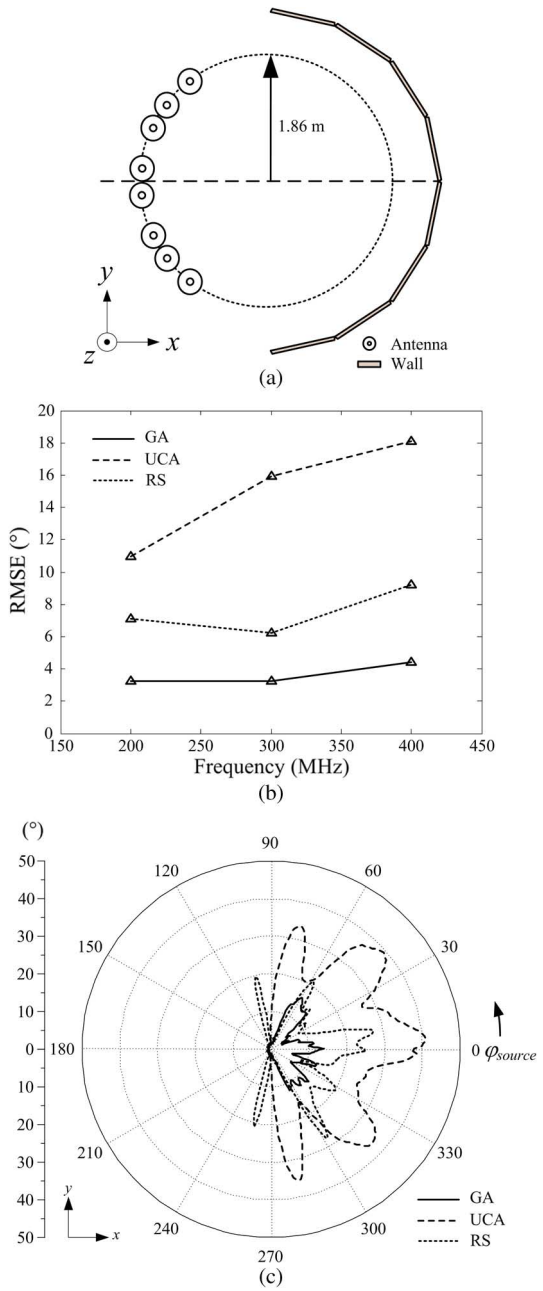

Fig. 5. Optimized results at $\varphi_{\mathrm{wall}} = 90°$. (a) Optimized antenna positions of GA. (b) RMSE versus frequency. (c) RMSE versus angles.

cording to source directions ($\varphi_{\mathrm{source}}$). When the source is located on the opposite side of the wall ($\varphi_{\mathrm{source}} = 180°$), the RMSE value is almost zero. However, it is raised significantly when the source is located in the direction of the platform, especially for the UCA. The GA consistently maintains a much lower RMSE, which is the main benefit of the optimum placement.

The optimized samples are next evaluated by their RMSE under multiple incident sources, as shown in Fig. 6(a). It is assumed that two sources exist in the azimuth direction, and their angular separation is defined as

$$\Delta\varphi_{\mathrm{source}} = |\varphi_{2\mathrm{nd}} - \varphi_{1\mathrm{st}}| \tag{8}$$

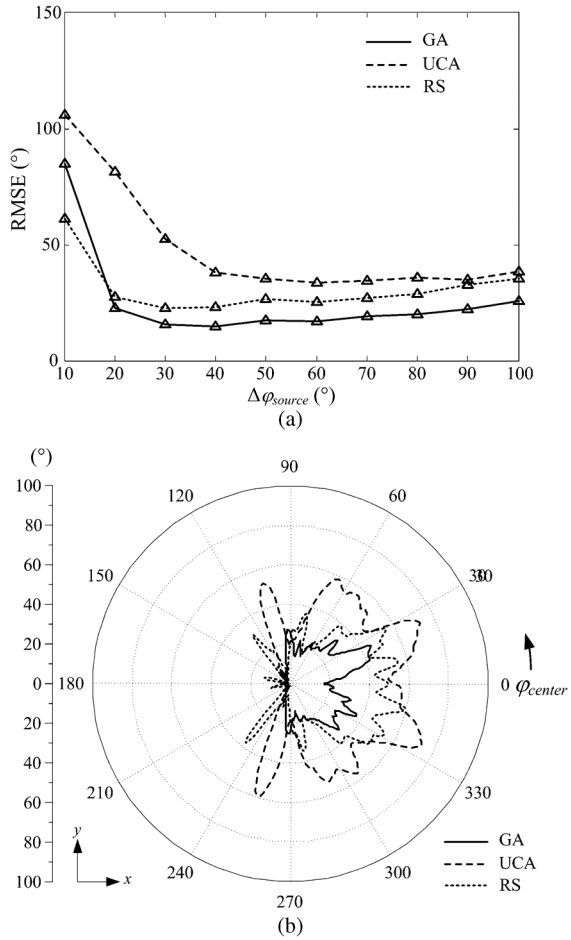

Fig. 6. Estimation of multiple incident angles. (a) RMSE versus $\Delta\varphi_{\mathrm{source}}$. (b) RMSE versus incident angle ($\Delta\varphi_{\mathrm{source}} = 50°$).

where $\varphi_{1\mathrm{st}}$ is the first source direction, and $\varphi_{2\mathrm{nd}}$ indicates the second source direction. The total RMSE of the two sources is defined as the sum of the RMSE for the first source and that of the second source. For this evaluation, $\Delta\varphi_{\mathrm{source}}$ is varied from 10° to 100° at intervals of 10°, and then the RMSE at each interval is averaged over the number of frequency points and the number of evaluated $\varphi_{1\mathrm{st}}$. As the value of $\Delta\varphi_{\mathrm{source}}$ increases, the RMSE of the UCA falls to approximately 40°, while the GA shows almost half the RMSE value of about 20°, which is lower than the RS result. In Fig. 6(b), the result of $\Delta\varphi_{\mathrm{source}} = 50°$ is chosen and further evaluated by the RMSE according to the center angle ($\varphi_{\mathrm{center}}$) of the sources, which is defined as

$$\varphi_{\mathrm{center}} = \varphi_{1\mathrm{st}} + \frac{\Delta\varphi_{\mathrm{source}}}{2} \tag{9}$$

Similar to what was observed in the single DOA estimation, the GA consistently maintains a lower RMSE for all source directions when compared to the RMSE results from the UCA and RS. From this set of results, we see that if a design has higher accuracy for the single DOA estimation, it is likely to have higher DOA accuracy under multiple sources.

D. Interpretation

In this section, the optimized antenna positions of the GA are compared with those of the UCA to examine how they bring

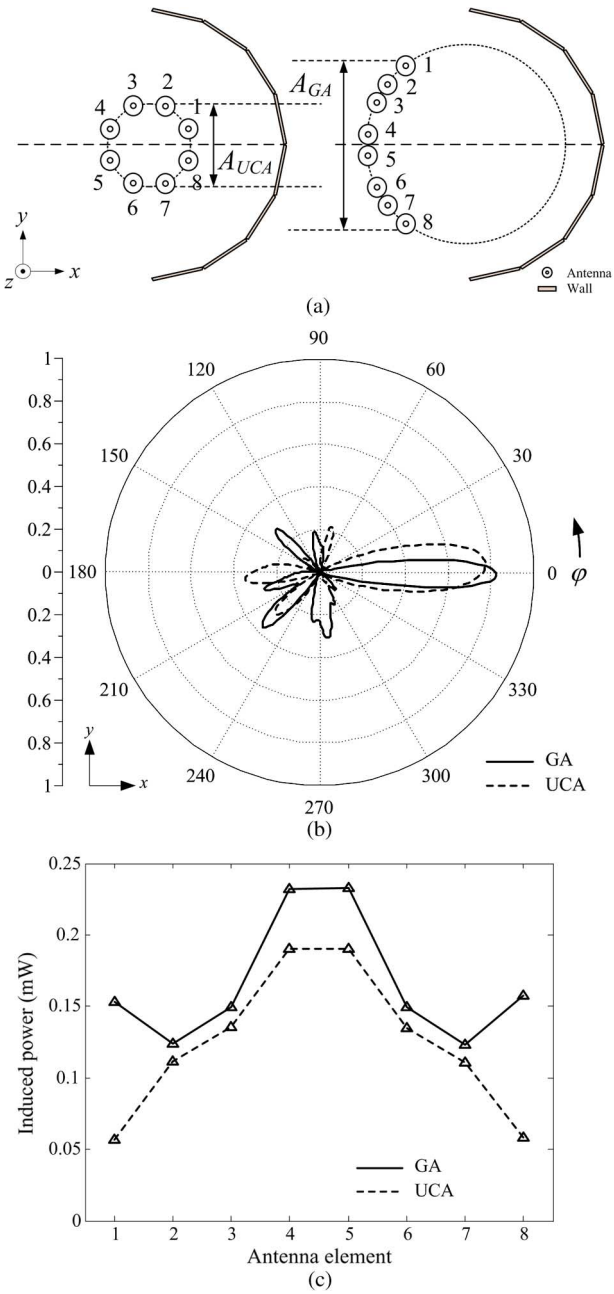

Fig. 7. Comparison of optimized results. (a) Aperture size and antenna numbers. (b) Power spectrum at 300 MHz. (c) Induced power on antenna elements.

about the RMSE improvement in the presence of strong platform effects. Fig. 7(a) shows the antenna positions of the UCA (left) and the GA (right) obtained when $\varphi_{\text{wall}} = 90°$. The effective aperture sizes of the two designs, defined as A_{UCA} and A_{GA}, are measured as specified in the figure. The measurement shows that A_{GA} is almost twice as large as A_{UCA} ($A_{\text{UCA}} = 1.42$ m and $A_{\text{UCA}} = 2.93$ m). Consequently, the spectrum width of the GA becomes sharper in the direction of the platform. Fig. 7(b) shows a comparison of the spectrum widths between the GA and the UCA in the case when the SNR is 5 dB and the source is located at $\varphi = 0°$. The figure shows asymmetric spectrums due to the random noise characteristics, although the arc-wall and the array configurations are symmetrical with respect to the x-axis. As can be seen, the GA shows a half-power spectrum width of 7.4°, which is smaller than the UCA (12.5°). In other words, a better resolution can be achieved in the platform direction when array elements are arranged on the other side of the platform.

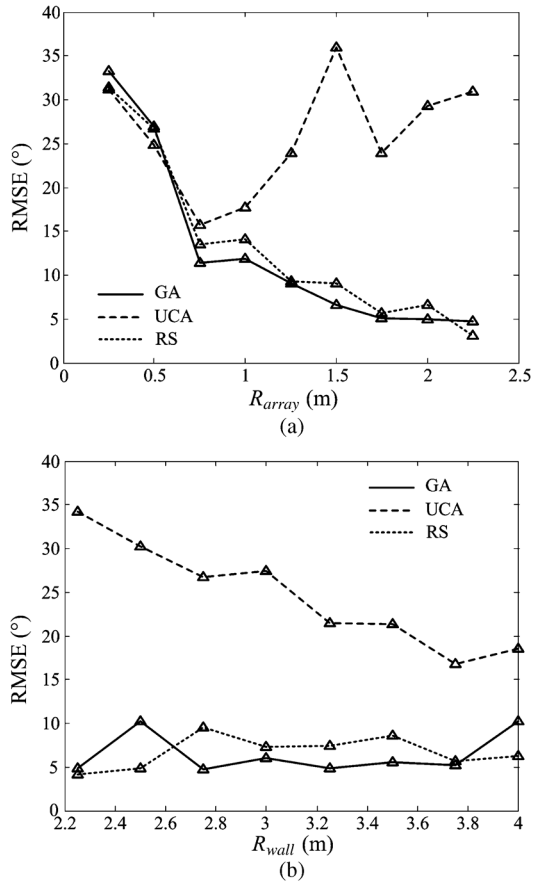

Fig. 8. Parametric study using arc-wall. (a) RMSE versus R_{array}. (b) RMSE versus R_{wall}.

We now observe the induced power level on each array element in Fig. 7(c). This observation is conducted to verify the RMSE improvement from the SNR perspective. The UCA result shows a minimum induced power level of 0.06 mW in elements 1 and 8 due to the proximity to the wall. On the other hand, the minimum induced power level of the GA is 0.12 mW, and thus the average induced power level of the GA design is raised by 0.05 mW as compared to that of the UCA. As a result, the SNR of the GA design is increased from 5.95 dB to 7.22 dB according to the following definition:

$$SNR = \frac{P_{\text{signal}}}{P_{\text{noise}}} \tag{10}$$

where P_{signal} is the signal power, and P_{noise} is the noise power. It is assumed that the antenna located at the center of the array has an SNR value of 10 dB in free space. Therefore, the increase in SNR provides another argument on why the position arrangement can improve the RMSE in the direction of the platform.

E. Parametric Study

Without further optimization, we examine the RMSE versus different values of R_{array} and R_{wall} using the already-optimized

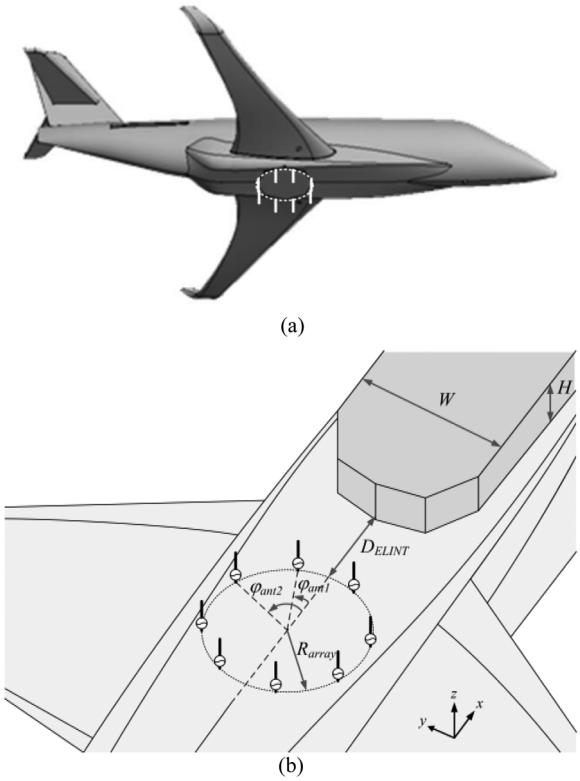

Fig. 9. Geometry and optimization parameters of aircraft. (a) Side bottom view. (b) Placement parameters.

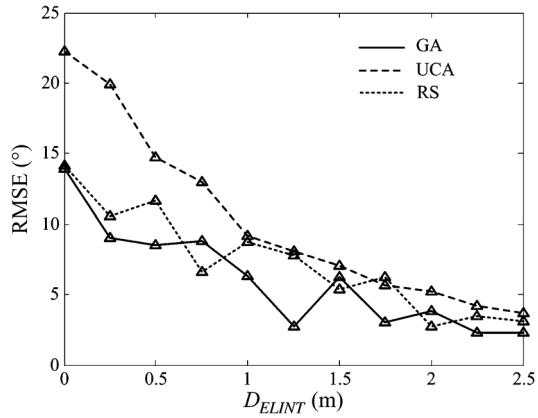

Fig. 10. Optimized RMSE according to D_{ELINT}.

TABLE II
OPTIMIZED RESULTS OF AIRCRAFT ($D_{\mathrm{ELINT}} = 1.25$ m)

Parameters	UCA	RS	GA
R_{array}	0.75 m	0.75 m	0.75 m
φ_{ant1}	22.5°	52°	70°
φ_{ant2}	67.5°	68°	94°
φ_{ant3}	112.5°	141°	125°
φ_{ant4}	157.5°	162°	160°
φ_{ant5}	202.5°	198°	200°
φ_{ant6}	247.5°	219°	235°
φ_{ant7}	292.5°	292°	266°
φ_{ant8}	337.5°	308°	290°

element positions. These two parameters are chosen because they are closely related to the aperture size and the average induced power level, which were identified as the reason for the performance improvement in the last section. Fig. 8(a) shows the RMSE versus R_{array} when R_{wall} is fixed at 2.5 m. The RMSE decreases as the value of R_{array} increases, except for the UCA. Although the UCA shows an RMSE improvement up to 0.75λ at 300 MHz due to the increased aperture size, its RMSE is rapidly increased due to the onset of grating lobes when the element spacing is larger than half a wavelength. Fig. 8(b) shows the RMSE for different values of R_{wall}. As expected, the UCA shows improvement as the wall moves farther away from the array elements. Nevertheless, its RMSE value is higher for the entire range of R_{wall} as compared to the GA and the RS, whose values stay consistently at around 5°.

III. Application to Military Aircraft

A. Geometry

Our approach is now extended to a realistic military aircraft model, which usually includes a protruding structure near the antenna array, as shown in Fig. 9(a). In our simulation, a model of the Gulfstream G200 is imported as 35,796 piecewise mesh triangles, having an overall size of 18.9 m × 17.5 m × 5.8 m. At the bottom of this model, there is an electronic "ELINT" device whose length (L), width (W), and height (H) are 5.0 m, 1.6 m, and 0.5 m, respectively. This device usually contains a metal structure inside the radome. However, for simplicity, the structure as well as the entire aircraft is assumed to be perfectly conducting. We vary the distance from the 'ELINT' device to the array, denoted as D_{ELINT}, to change the strength of the platform effects. Fig. 9(b) shows the bottom view of the aircraft with eight quarter-wavelength monopole antennas arranged by their angular coordinates around a circle of radius R_{array}. We fix the value of R_{array} at 0.75 m to fit within the aircraft fuselage, whose width is only about 1.6 m.

B. Optimum Placement

Fig. 10 shows the optimized RMSE values according to the distance D_{ELINT}. The UCA result decreases monotonically from 22.3° to 3.7° as D_{ELINT} is increased. The GA consistently maintains a lower RMSE value as compared to the UCA. The most significant improvement is found at $D_{\mathrm{ELINT}} = 1.25$ m, with an RMSE value of 2.7°, which is almost three times lower than that of the UCA.

Table II shows the optimized parameters in the case of $D_{\mathrm{ELINT}} = 1.25$ m, and Fig. 11(a) presents the optimized antenna positions of the GA. As we have observed previously in the arc-wall case, the antennas are arranged on the opposite side of the scattering object to increase the DF accuracy. Fig. 11(b) shows the RMSE in the operating frequency range, and it verifies that the GA result brings consistent RMSE improvement over the entire frequency range. We then examine the RMSE according to $\varphi_{\mathrm{source}}$, as shown in Fig. 11(c). The RMSE of the UCA is raised to the value of 42.6° by platform effects in the direction of the 'ELINT' device $(\varphi_{\mathrm{source}} = 0°)$; however, the GA shows an almost six times lower RMSE of 7.2°.

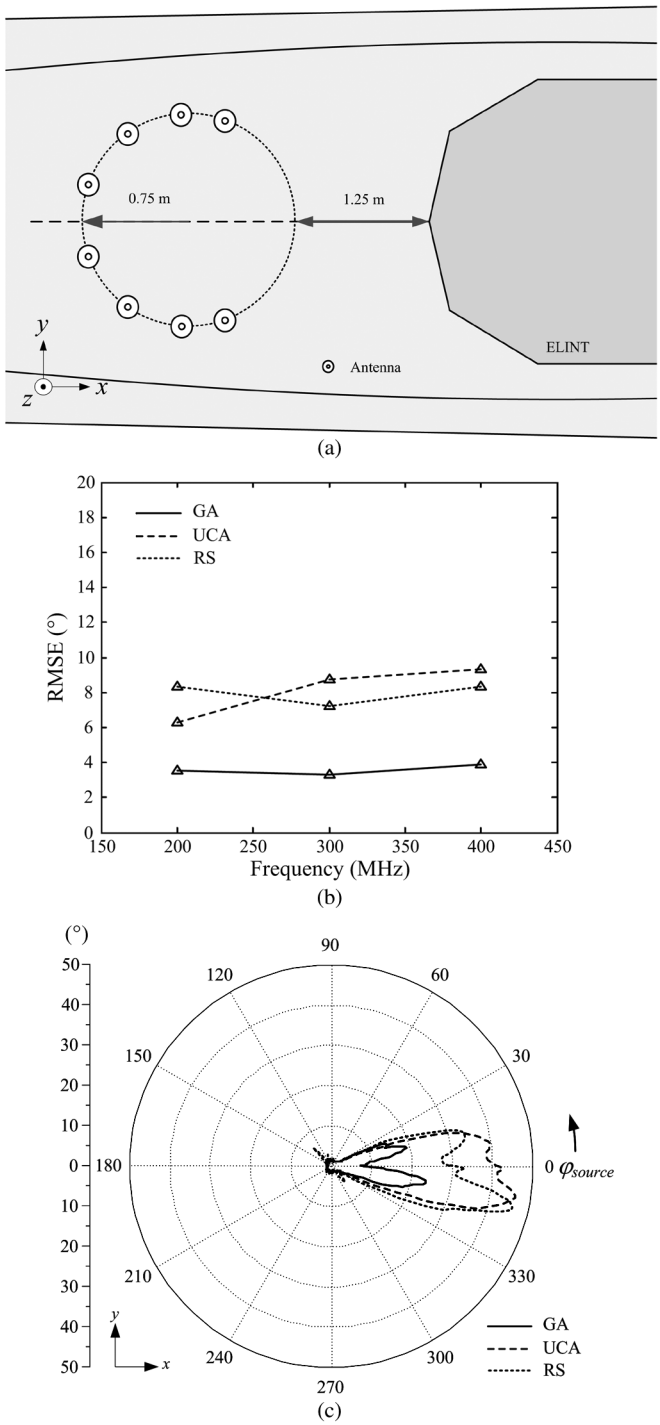

Fig. 11. Optimized results at $D_{\mathrm{ELINT}} = 1.25$ m. (a) Optimized antenna positions of GA. (b) RMSE versus frequency. (c) RMSE versus incident angle.

The optimized samples are also evaluated through the RMSE in the case of multiple incoming signals by using the same approach as that for the arc-wall case. Fig. 12(a) represents the RMSE according to $\Delta\varphi_{\mathrm{source}}$. As the value of $\Delta\varphi_{\mathrm{source}}$ increases, the RMSE of the UCA falls to about 25.9°, while that of the GA has a value of 11.9°, which is lower by half. The RMSE versus $\varphi_{\mathrm{center}}$ for $\Delta\varphi_{\mathrm{source}} = 50°$ is plotted in Fig. 12(b). When the source is in the direction of the 'ELINT' device, the RMSE of the UCA sharply increases to the maximum value of about

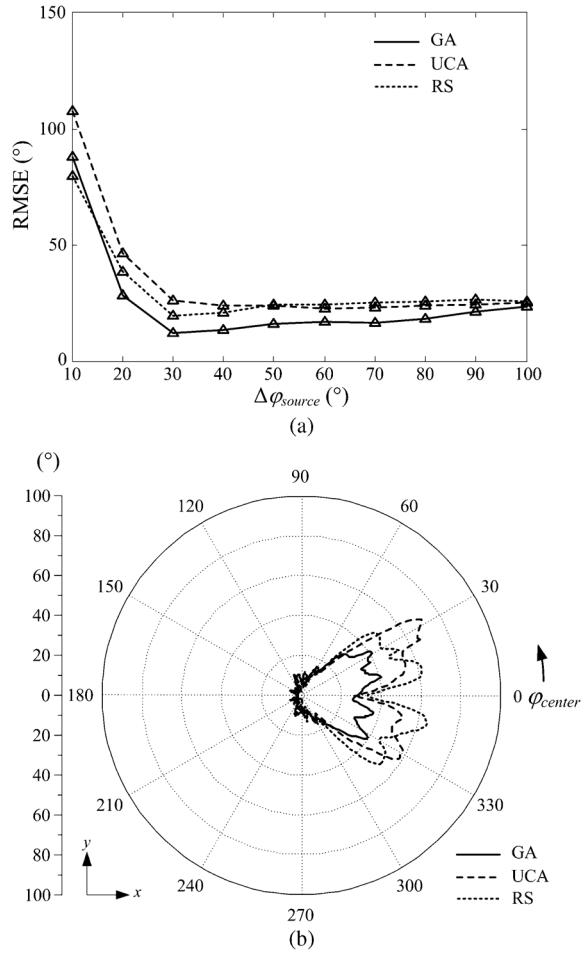

Fig. 12. Estimation of multiple incident angles on aircraft. (a) RMSE versus $\Delta\varphi_{DOA}$. (b) RMSE versus incident angle ($\Delta\varphi_{DOA} = 50°$).

70°, but the GA consistently maintains an almost 50% lower RMSE value of about 30°.

C. Parametric Study

To determine the size limitation of the 'ELINT' device, we set the maximum tolerable RMSE value to 3°, which is the typical requirement for the DF system installation on aircraft. The size of the device is adjusted by the width W and the height H, whose nominal sizes are 1.6 m and 0.5 m, respectively. It is assumed that the array is placed at $D_{\mathrm{ELINT}} = 1.25$ m, and the element positions are optimized by the use of our optimization process for every device size using both the UCA and non-UCA (GA and RS, respectively) configurations. Fig. 13(a) shows the variation of the optimized RMSE according to the width W varying from 0.4 m to 2.0 m, while the height H is fixed at its nominal size of 0.5 m. As can be seen in the figure, the RMSE value can be maintained at less than 3°, when $W \leq 0.8$ m for the UCA and $W \leq 1.6$ m for the GA. Fig. 13(b) shows another RMSE variation according to the height H. In this simulation, W is fixed at 1.6 m, while H varies from 0.125 m to 0.625 m. The result shows that H should be smaller than 0.375 m for the UCA and smaller than 0.5 m for the GA.

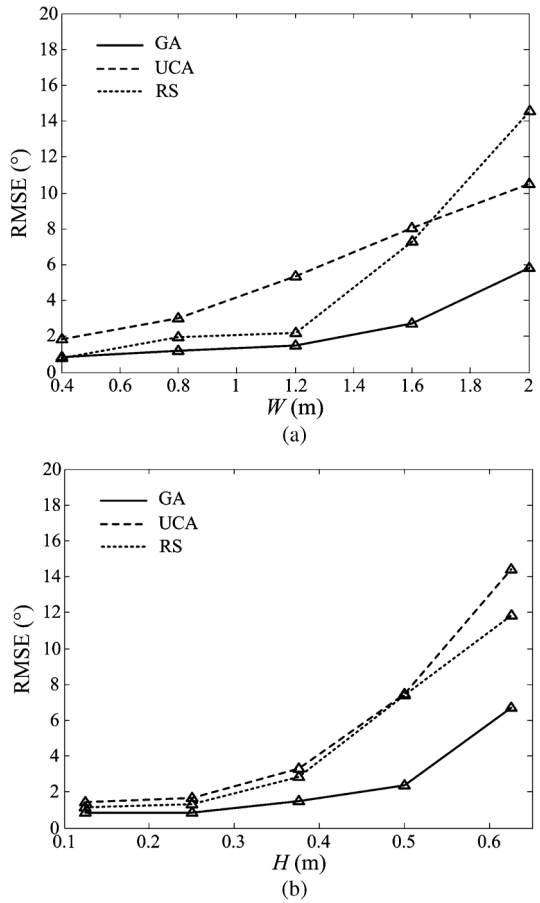

Fig. 13. RMSE according to 'ELINT' size. (a) RMSE versus W. (b) RMSE versus H.

IV. Conclusion

We have investigated a systematic approach for DF antenna placement in a harsh platform environment. To study the influence of the platform, we first introduced a generic arc-wall structure, in which the strength of the platform effects can be controlled by the radius and angular extent of the wall. We then moved on to a more realistic aircraft having the strong scattering 'ELINT' object. In our approach, the signal-subspace MUSIC algorithm was used to calculate the average RMSE over all azimuth angles. Eight omni-directional elements were used in the circular array, and their positions were defined by their coordinates around the circle. Detailed parameters were optimized by using the GA in conjunction with the FEKO EM simulator. The optimized result in the arc-wall case ($\varphi_{\text{wall}} = 90°$) showed an RMSE value of 3.6° (GA), which is almost four times lower than the UCA (15.0°). We also observed the RMSE improvement from 8.0° (UCA) to 2.7° (GA) in the aircraft application ($D_{\text{ELINT}} = 1.25$ m). We verified that this RMSE improvement was achieved by the element positions, arranged on the opposite side of the platform, which makes the spectrum width sharper and raises the SNR in the platform direction. The results obtained in this paper demonstrate that by properly optimizing array element positions, it is possible to achieve accurate DOA estimation in a harsh platform environment.

References

[1] C. A. Balanis, *Antenna Theory: Analysis and Design*, 3rd ed. Hoboken, NJ, USA: Wiley, 2005.
[2] E. R. Ferrara, Jr. and T. M. Parks, "Direction finding with an array of antennas having diverse polarizations," *IEEE Trans. Antennas Propag.*, vol. 31, no. 2, pp. 231–236, Mar. 1983.
[3] J. Li, "Direction and polarization estimation using arrays with small loops and short dipoles," *IEEE Trans. Antennas Propag.*, vol. 41, no. 3, pp. 379–387, Mar. 1993.
[4] A. J. Paulraj and C. B. Papadias, "Space-time processing for wireless communications," *IEEE Signal Process. Mag.*, vol. 14, no. 6, pp. 49–83, Nov. 1997.
[5] I. J. Gupta and A. A. Ksienski, "Effect of mutual coupling on the performance of adaptive arrays," *IEEE Trans. Antennas Propag.*, vol. AP-31, no. 9, pp. 785–791, Sep. 1983.
[6] D. F. Kelley and W. L. Stutzman, "Array antenna pattern modeling methods that include mutual coupling effects," *IEEE Trans. Antennas Propag.*, vol. 41, no. 12, pp. 1625–1632, Dec. 1993.
[7] K. R. Dandekar, H. Ling, and G. Xu, "Effect of mutual coupling on direction finding in smart antenna applications," *Electron. Lett.*, vol. 36, no. 22, pp. 1889–1891, Oct. 2000.
[8] Q. Bao, C. C. Ko, and W. Zhi, "DOA estimation under unknown mutual coupling and multipath," *IEEE Trans. Aerosp. Electron. Syst.*, vol. 41, no. 2, pp. 565–573, Apr. 2005.
[9] B. Friedlander and A. J. Weiss, "Direction finding in the presence of mutual coupling," *IEEE Trans. Antennas Propag.*, vol. 39, no. 3, pp. 273–284, Mar. 1991.
[10] B. C. Ng and C. M. S. See, "Sensor-array calibration using a maximum-likelihood approach," *IEEE Trans. Antennas Propag.*, vol. 44, no. 6, pp. 827–835, Jun. 1996.
[11] R. Adve and T. Sarkar, "Compensation for the effects of mutual coupling on direct data domain adaptive algorithms," *IEEE Trans. Antennas Propag.*, vol. 48, no. 1, pp. 86–94, Jan. 2000.
[12] F. Obelleiro, L. Landesa, J. M. Taboada, and J. L. Rodriguez, "Synthesis of onboard array antennas including interaction with the mounting platform and mutual coupling effects," *IEEE Antennas Propag. Mag.*, vol. 43, no. 2, pp. 76–82, Apr. 2001.
[13] K. R. Dandekar, H. Ling, and G. Xu, "Experimental study of mutual coupling compensation in smart antenna applications," *IEEE Trans. Wireless Commun.*, vol. 1, no. 3, pp. 480–487, Jul. 2002.
[14] H. T. Hui, "Improved compensation for the mutual coupling effect in a dipole array for direction finding," *IEEE Trans. Antennas Propag.*, vol. 51, pp. 2498–9–2503, Sep. 2003.
[15] T. Su and H. Ling, "Array beamforming in the presence of a mounting tower using genetic algorithms," *IEEE Trans. Antennas Propag.*, vol. 53, no. 6, pp. 2011–2019, Jun. 2005.
[16] FEKO Suite 6.1, EM Software and Systems, 2012 [Online]. Available: http://www.feko.info
[17] R. O. Schmidt, "Multiple emitter location and signal parameter estimation," *IEEE Trans. Antennas Propag.*, vol. AP-34, no. 3, pp. 276–280, Mar. 1986.
[18] H. Krim and M. Viberg, "Two decades of array signal processing research: The parametric approach," *IEEE Signal Process. Mag.*, pp. 67–94, Jul. 1996.
[19] A. L. Swindlehurst and T. Kailath, "A performance analysis of subspaced-based methods in the presence of model errors, Part I: The MUSIC algorithm," *IEEE Trans. Signal Process.*, vol. 40, no. 7, pp. 1758–1774, Jul. 1992.
[20] C. P. Mathews and M. D. Zoltowski, "Eigenstructure techniques for 2-D angle estimation with uniform circular arrays," *IEEE Trans. Signal Process.*, vol. 42, no. 9, pp. 2395–2407, Sep. 1994.
[21] Y. Rahmat-Samii and E. Michielssen, *Electromagnetic Optimization by Genetic Algorithms*. Hoboken, NJ, USA: Willey, 1999.

Gangil Byun (S'12) was born in Seoul, Korea, in 1984. He received the B.S. and M.S. degrees in electronic and electrical engineering from Hongik University, Seoul, Korea, in 2010 and 2012, respectively. He is currently pursuing the Ph.D. degree in electronics and computer engineering at Hanyang University, Seoul, Korea.

His research interests include the design of aircraft antennas, global positioning system antennas, antenna arrays, and position optimization of array elements for adaptive beamforming applications.

Hosung Choo (S'00–M'04–SM'11) was born in Seoul, Korea, in 1972. He received the B.S. degree in radio science and engineering from Hanyang University, Seoul, Korea, in 1998, and the M.S. and Ph.D. degrees in electrical and computer engineering from the University of Texas, Austin, TX, USA, in 2000 and 2003, respectively.

In September 2003, he joined the school of electronic and electrical engineering, Hongik University, Seoul, Korea, where he is currently an Associate Professor. His principal areas of research are the use of the optimization algorithm in developing antennas and microwave absorbers. His studies include the design of small antennas for wireless communications, reader and tag antennas for RFID, and on-glass and conformal antennas for vehicles and aircraft.

Hao Ling (S'83–M'86–SM'92–F'99) received the B.S. degrees in electrical engineering and physics from the Massachusetts Institute of Technology, Cambridge, MA, USA, in 1982, and the M.S. and Ph.D. degrees in electrical engineering from the University of Illinois at Urbana-Champaign, Urbana, IL, USA, in 1983 and 1986, respectively.

He joined the faculty of the University of Texas, Austin, TX, USA, in September 1986 and is currently a Professor of electrical and computer engineering and holder of the L. B. Meaders Professorship in Engineering. His principal areas of research are in radar signature prediction and radar feature extraction. He has actively contributed to the development and validation of numerical and asymptotic methods for characterizing the radar signatures from complex targets. In 1986, he and his collaborators pioneered the shooting and bouncing ray (SBR) technique for predicting the radar returns from realistic aerospace vehicles. He was a co-developer of the SBR-based code *Xpatch*, which has been distributed to over 450 government and industrial organizations in the United States. *Xpatch* was an enabling technology in several radar target identification programs, including the U.S. Air Force Non-Cooperative Target Identification Program and DARPA's Moving and Stationary Target Acquisition and Recognition Program. His recent research interests also include radar signal processing, radar sensing of humans, miniaturized and broadband antenna design, and propagation channel modeling in non-line-of-sight environments. His research activities have been funded by the NSF, ONR, AFRL, AFOSR, DARPA, DOE, and NASA, as well as aerospace companies including Lockheed, Boeing, and Northrop. He has published 190 journal papers and 210 conference papers to date and coauthored a book on radar imaging (Artech House, 2002).

Dr. Ling received the National Science Foundation Presidential Young Investigator Award in 1987, the NASA Certificate of Appreciation in 1991, the University of Illinois Distinguished Alumni Award in 2009, and several teaching awards from the University of Texas. He served on a number of U.S. and NATO panels on high-resolution SAR and ISAR imaging, including the NATO Sensors and Electronics Technology Panel and the Naval International Cooperative Opportunities in Science and Technology program. He was a guest editor of a 2003 special issue on time-frequency analysis for synthetic aperture radar and feature extraction for the *IEE Proceedings on Radar, Sonar and Navigation*.